scientific reports

Check for updates

OPEN

Subject-specific biomechanics influences tendon strains in patients with Achilles tendinopathy

Alessia Funaro[1]✉, Vickie Shim[2], Ine Mylle[1] & Benedicte Vanwanseele[1]

The treatment of Achilles tendinopathy is challenging, as 40% of patients do not respond to existing rehabilitation protocols. These protocols neglect individual Achilles tendon (AT) characteristics, which are crucial for healing of the tendon tissue. Although prior studies suggest an optimal strain for AT regeneration (6% tendon strains), it is unclear if current protocols meet this condition. Our study aimed to analyse the impact of a selection of rehabilitation exercises on tendon strains in patients with Achilles tendinopathy, using subject-specific finite element (FE) models of the free AT. Second, this study aimed to explain the influence of muscle forces and material properties on AT strains. The 21 FE models of the AT included the following subject-specific features: geometry estimated from 3D freehand ultrasound images, Elastic modulus estimated from the experimental stress–strain curve, and muscle forces estimated using a combination of 3D motion capture and musculoskeletal modelling. Exercises were ranked based on strain progression, starting from concentric and eccentric exercises, and going to more functional exercises, which impose a greater load on the AT. There was no significant difference between the unilateral heel drop and walking, and both exercises fell within the optimal strain range. However, when examining individual strains, it became evident that there was diversity in exercise rankings among participants, as well as exercises falling within the optimal strain range. Muscle forces notably affected strains more than material properties. Our findings indicate the importance of tailored rehabilitation protocols that account for individual morphological, material, and muscle characteristics.

Keywords Achilles tendon, Twisting sub-tendon morphology, Subject-specific 3D models, Tendon strains, Finite element modelling, Rehabilitation exercises

Achilles tendinopathy is a multifaceted condition[1] that can profoundly affect individuals[2], including both athletes and those with relatively low levels of physical activity[3]. Degenerative changes usually occur in the mid-portion of the free Achilles tendon (AT)[4], with pain as the main symptom. For this reason, the current rehabilitation protocols aim to reduce aggravating loads by introducing pain-relieving loads[5]. At present, rehabilitation protocols tend to include a variety of exercises, namely, eccentric exercises[6], a combination of eccentric and concentric exercises[7] and a combination of more functional exercises[8]. Although eccentric muscle training is the preferred choice for decreasing pain in patients with chronic Achilles tendinopathy[7], there is still little clinical or mechanistic evidence for the isolation of the eccentric component[9]. Previous animal studies have demonstrated that a certain loading regime (and consequently tendon strains: 6%) promotes tendon remodelling and the creation of a proper (internal) mechanical environment and therefore is able to reverse early-stage pathological changes in patients with Achilles tendinopathy[10]. Additionally, in healthy humans, a specific threshold of strain magnitude (~5%) must be reached to initiate adaptive changes in both the mechanical and morphological characteristics of the AT[11]. However, it remains unknown whether current rehabilitation exercises provide the optimal strain dose needed for tendon adaptation and regeneration. Indeed, Achilles tendinopathy treatment is still challenging, and the failure rate of classical treatment schemes is still high, with 40% of patients not responding to these types of training[12].

The morphology and material properties of tendinopathic tendons are influenced by changes in tissue structure, such as the disruption of collagen fibre structure and arrangement and increased type III collagen content[13,14]. Indeed, previous investigations have demonstrated that morphological and material changes, including increased cross-sectional area (CSA) and reduced stiffness and Young's modulus, are observable

[1]Human Movement Biomechanics Research Group, Department of Movement Sciences, KU Leuven, Leuven, Belgium. [2]Auckland Bioengineering Institute, University of Auckland, Auckland, New Zealand. ✉email: alessia.funaro@kuleuven.be

Content courtesy of Springer Nature, terms of use apply. Rights reserved

in patients with tendinopathy compared to healthy individuals[15]. In the aforementioned study, experimental data of tendon force and elongation were used for the estimation of tendon strain. However, this experimental measure does not take into account the complex subject-specific geometry of the AT, which makes it unsuitable for investigating internal tendon strains. The AT is the junction of three independent tendons arising from the triceps surae muscles (from the soleus (SOL), gastrocnemius medialis (GM) and lateralis (GL)). Hence, three sub-tendons (SOL, GM, and GL, respectively) are fused together in the AT, following the typical twisting structure of the AT. Shim et al.[16] demonstrated that the presence of a twist enables a more uniform distribution of stress across the AT when subjected to differential forces from the triceps surae muscles. Different twisted morphologies were observed among individuals[17], with the least twisted configuration being predominant[18]. Hence, it is essential to account for this twisted geometry to better understand the distribution of stress (and strain) within the AT under load, which reflects the key morphological features observed in individuals. Moreover, the differential force exerted by the triceps surae muscles plays a crucial role in the elongation of the sub-tendons and subsequently in the strain in the AT. In patients with Achilles tendinopathy, there is a noticeable change in the force distribution strategies employed by the triceps surae muscles during dynamic tasks[19]. Consequently, it is pivotal to consider the impact of triceps surae muscle forces on AT when examining the factors contributing to strain distribution in patients with Achilles tendinopathy.

Our previous study[20] showed that finite element (FE) models of the AT can be used to estimate internal tendon strains during rehabilitation exercises, especially under the influence of varying tendon geometry and material properties. Yin et al.[21] showed how different AT morphologies experience different stress and strain distributions, implying that the injury risk varies among individuals. Moreover, Hansen et al.[22] and Shim et al.[23] noted that free AT stress is highly dependent on subject-specific tendon geometry. Additionally, each individual possesses unique material properties[21]. These combined findings suggest that personalized geometry and material properties are essential features that should be included in AT FE models when investigating tendon strains during dynamic exercises, especially in patients with Achilles tendinopathy. Previous AT FE studies that incorporated subject-specific geometry and material properties mainly used data from healthy individuals, which do not account for the altered AT geometry and material properties that are typical of patients with Achilles tendinopathy. When altered AT material and geometry in patients with Achilles tendinopathy were considered[24], the number of developed FE models was lower ($n=8$), and the models did not include sub-tendons. Additionally, muscle forces boundary conditions were recorded during a maximum voluntary isometric contraction (MVC) and not during dynamic conditions, such as rehabilitation exercises. Devaprakash et al.[25] demonstrated that estimates of AT strain vary significantly depending on the specific rehabilitation tasks undertaken. Nevertheless, the strain in the AT was determined in a healthy cohort using external measures that did not consider the tendon's geometry or material properties. Consequently, these external measures are inadequate for describing the internal load on the tendon, which is more suitable for FE analysis. In fact, little is known about the influence that subject-specific muscle forces have on AT strains in patients with Achilles tendinopathy.

The primary objective of this study was to apply a previously developed pipeline, as outlined in Funaro et al.[20], within a clinical population to assess how various rehabilitation exercises impact tendon strains in patients with Achilles tendinopathy. The goal was to rank these exercises based on the average strain observed in the mid-portion of the AT. Moreover, we aimed to explore the individual differences in tendon strains during different rehabilitation exercises in patients with Achilles tendinopathy and to explain the influence of muscle forces and material properties on the AT strain. To do this, we developed subject-specific FE models of 21 patients with Achilles tendinopathy, which included subject-specific geometry, material properties and muscle forces during commonly used rehabilitation exercises. We hypothesized that the strains are lower in concentric and eccentric exercises and gradually increase in more functional exercises in patients with Achilles tendinopathy. Finally, we also wanted to determine whether strains in the subject-specific FE models are more correlated with subject-specific muscle forces rather than with subject-specific material properties.

Materials and methods

Participants characteristics

Twenty-one patients with mid-portion Achilles tendinopathy (17 males, 4 females; age: 49 ± 13 years, height: 178 ± 8 cm, weight: 75 ± 12 kg, average $\pm$ SD) participated in the study. The participants met the following inclusion criteria: (I) a history of intermittent episodes of AT pain lasting more than six consecutive weeks within the past five years; (II) more than one episode of tendon pain exacerbation and remission within the past five years; (III) palpable focal thickening of the AT in the mid-substance; (IV) pain originating from the AT on palpation of thickened AT; and (V) sonographic evidence of tendinopathy. Patients with Achilles tendinopathy were excluded from the study if they reported any of the following: (I) history of previous surgery or tears involving the AT; (II) systemic diseases affecting collagenous tissue; or (III) insertional Achilles tendinopathy, calcaneal spurs, plantar fasciitis, or other conditions affecting the foot and ankle complex. All participants completed the Victorian Institute of Sport Assessment-Achilles questionnaire (VISA-A)[26], which provides an index of Achilles tendinopathy pain and function (VISA-A score: 73 ± 19). The study was approved by the Ethics Committee Research of UZ/KU Leuven, and all relevant ethical guidelines, including the provision of written informed consent prior to participation in the study, were followed. The study was performed based on the guidelines formulated in the Declaration of Helsinki.

Experimental data

Data collection

The data were collected from patients with Achilles tendinopathy after a clinical examination and before starting the rehabilitation program so that all participants were evaluated at the same stage. Participants were asked to lie prone on an isokinetic dynamometer (Biodex Medical Systems, Shirley, New York, USA) with their knee and

Content courtesy of Springer Nature, terms of use apply. Rights reserved

hip fully extended, with a fixated foot and a neutral ankle angle. The protocol started with a familiarization of the plantarflexion task and a standardized warm-up. Each participant performed two repetitions of a 5 s MVC. A rest period of 120 s was allowed between contractions. The MVC was repeated if the difference between the contractions was > 8%. After applying a 150 ms moving average, the contraction with the highest torque on the tendinopathic side was chosen to determine the target torque (30% and 60% MVC) in the subsequent testing task.

During this second task, 3D free-hand ultrasound (3DfUS) images were acquired during resting condition and isometric contractions at 30% and 60% MVC. A conventional 2D ultrasound machine with a 40-mm linear transducer (L15-7H40-A5, ArtUs EXT-1 H system, UAB Telemed, Vilnius, Lithuania) was used to record images of the AT. The ultrasound machine was combined with an optical motion tracking system (V120:Trio tracking system, Optitrack, Corvallis, OR, USA) to generate a 3D reconstruction of the AT. First, the AT of the participants was scanned during the resting condition. These images were used for the generation of the subject-specific mesh. Afterwards, the participants performed six contractions to reach a torque of 30% and 60% of the MVC (three contractions for each condition, randomized order). Fatigue was monitored by maintaining a 120 s resting time between contractions. Pain was monitored by asking the participant to give a pain score between 1 and 10. The feedback of the torque was provided via visual feedback displayed on a monitor in front of the participant.

Subsequently, the linear probe was placed longitudinally over the AT to acquire a static ultrasound image at rest, with the centre of the probe aligned with the centre of rotation (COR), which is the inferior tip of the lateral malleolus of the tendinopathic ankle. The distance from the inferior tip of the US probe to the COR was measured using a tape measure (d_1)[27]. This measure was subsequently used for the estimation of the moment arm, as described in the following section. The moment arm was necessary to calculate the force value from the MVC, which was used for the estimation of the Elastic modulus (E).

Estimation of subject-specific Elastic modulus (E)

The subject-specific E was estimated using 3DfUS experimental data. All 3DfUS images were segmented with 3D Slicer (version 4.11.20210226) software. To determine the subject-specific tendon length, two main anatomical landmarks (the calcaneal notch and soleus muscle-tendon junction) were manually located on 2D images of the AT, and the tendon length was defined as the point-to-point distance between these two landmarks. Tendon elongation was calculated for both 30% and 60% MVC by subtracting tendon lengths in the two contractions from the corresponding resting length, which was used to calculate the overall tissue strain for each subject by dividing the subject's tendon elongation by the subject's resting length. Then, the subject-specific tendon force was calculated by dividing the subject-specific MVC by the subject-specific moment arm of the AT. The subject-specific moment arm was estimated from 2D images. First, the distance between the skin and midline of the AT (d_2), also known as the line of action[28], was measured. The difference between d_1 (explained in the Data collection section) and d_2 represented the AT moment arm[27]. Based on the findings of Raiteri et al.[29], no torque correction was applied to account for co-contraction during torque estimation. Tendon cross-sections were manually digitized from 3D images at a half distance between the calcaneal notch and the soleus muscle-tendon junction to estimate the subject-specific average CSA of the mid-portion of the AT. CSA was estimated at rest and at 30% and 60% MVC. Subject-specific tendon stress was then obtained by dividing the calculated subject-specific tendon force by the subject-specific CSA of the tendon. Finally, the subject-specific E was calculated as the slope of the line fitted to the subject-specific stress–strain values at 30% and 60% of the peak force for each subject. The subject-specific values of the E can be found as Supplementary Table S1. The average values and the standard deviations of the MVC, CSA at rest and E among the 21 participants can be found in Table 1.

Estimation of subject-specific muscle forces

The participants came for a second time to the Movement and posture Analysis Laboratory Leuven (Belgium) to complete five repetitions of six rehabilitation exercises in a randomized order: walking (walk), bilateral heel rise (birise), bilateral heel drop with extended knee (bidrop), unilateral heel drop with extended knee (unidrop), unilateral heel drop with flexed knee (unidrop bent) and bilateral hopping (bihop). Between trials, the participant was given a minimum of 30 s of rest before moving on to the next trial. An extended Plug-in Gait marker set including 34 retroreflective markers, of which trajectories were recorded using 10 infrared cameras (Vicon, Oxford Metrics, Oxford, United Kingdom) at a sampling rate of 150 Hz, was placed on anatomical landmarks to obtain kinematic data. Ground reaction force data were measured from the participant's affected leg using a force plate embedded in the walkway. During the exercises, the activity of the three triceps surae muscles was recorded using surface EMG (Zerowire). The EMG signals were normalized to ground contact time to align the modelled muscle activations with the experimental muscle activations, serving as validation for the modelled muscle activation. A modified generic musculoskeletal model (the OpenSim gait2392 model)[30] with six degrees of freedom and 43 Hill-type muscle-tendon actuators per leg was scaled in OpenSim 3.3 (OpenSim, Stanford, CA, United States), and joint kinematics were then computed using a Kalman Smoothing algorithm[31]. Next, an inverse dynamic approach was used to calculate the joint moments. The muscle-tendon dynamics of the

MVC (Nm)	Moment arm (mm)	CSA (mm^2)	E (MPa)
113 ± 32	45 ± 5	112 ± 31	632 ± 201

Table 1. The table shows the average of the subject-specific values for the maximum voluntary contraction (MVC), moment arm, cross-sectional area (CSA) and E.

Content courtesy of Springer Nature, terms of use apply. Rights reserved

43 Hill-type lower-limb muscle-tendon actuators in the musculoskeletal model, including muscle-tendon unit lengths and moment arms, were obtained using OpenSim's muscle analysis tool. These dynamics, along with experimentally measured joint angles and joint moments, were utilized as inputs for the optimization method. Using a dynamic optimization method, the muscle redundancy problem[32] was solved by minimizing the sum of the squared muscle activations to estimate the forces of the three triceps surae muscles (SOL, GM, and GL muscle forces). The subject-specific muscle forces at the time of peak total muscle force during each exercise were used as boundary conditions in the subject-specific FE models. The subject-specific values of the muscle forces can be found as Supplementary Table S2.

Generation of FE models

Development of the three types of AT FE models

For each participant, three FE models of the AT were developed. The first model, which we call the "*subject-specific model*", was developed with subject-specific geometry, material properties and muscles forces to determine the individual ranking of the exercises based on AT strains. Subsequently, to investigate the impact that subject-specific material properties and muscle forces have on AT strains, two additional models were developed. The first model, called the "*material model*", had a subject-specific E and generic muscle forces. The other model, called the "*muscle forces model*", had subject-specific muscle forces and generic E. The generic muscle forces were estimated as the average of the subject-specific muscle forces for each exercise (Table 2) among all the participants. The generic E was estimated as the average of the subject-specific E values (Table 1) among all the participants. All the models had subject-specific geometry. A summary of the characteristics of the three models is presented in Fig. 1.

Generic model geometry

A first generic template mesh was developed to allow for the consistent definition of the three sub-tendons within subject-specific FE models. This mesh was generated from an initial geometry obtained by segmentation of images from one healthy male subject (age = 22 years, weight = 64 kg, height = 180 cm) recorded by 3DfUS images, defining the outer geometry of the tendon. The tendon model was developed using Materialise 3-matic (Materialise NV, Leuven, Belgium). The mesh was divided into three sub-tendons and the twisting structure was defined. The ratio of the CSA of a particular sub-tendon to the whole AT mesh CSA, as well as the amount of twist, were not subject-specific but based on the measurements described by Pękala et al.[18]. In Pekala's study, the percentage of each sub-tendon's CSA relative to the entire AT's CSA was reported as follows: 43.59 ± 12.35% for the sub-tendon from the GL, 28.04 ± 10.04% for the sub-tendon from the GM, and 28.37 ± 9.78% for the sub-tendon from the SOL. In our study, we created only the least twisting geometry. This decision was based on its prevalence, as it is the most common type of twist observed in the population, occurring in 48.1% of cases[18]. Additionally, our earlier research indicated that the average strain in the mid-portion of the AT models is not influenced by the twist of the sub-tendons[20]. The sub-tendons geometries were meshed into 8-node hexahedral solid elements. A mesh convergence study was performed to refine the mesh until the Principal Effective Lagrange strains reached an asymptote.

Constitutive models

The geometry was represented as an incompressible, transversely isotropic hyperelastic material[33], which we used in our previous study[20]. The uncoupled strain energy function *(1)* can be written as follows:

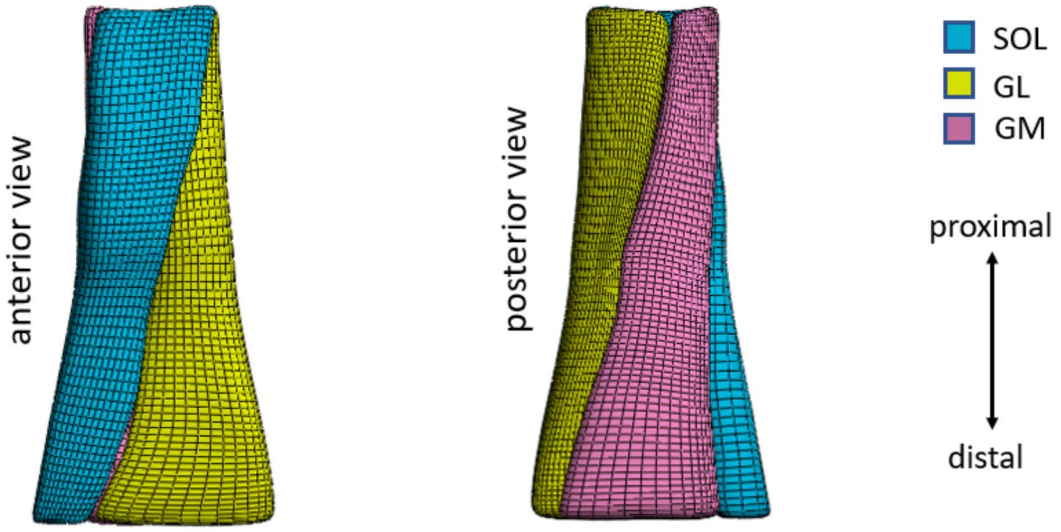
$$\boldsymbol{\Psi} = \boldsymbol{F}_1(\tilde{\boldsymbol{I}}_1, \tilde{\boldsymbol{I}}_2) + \boldsymbol{F}_2\left(\tilde{\boldsymbol{\lambda}}\right) + \frac{\boldsymbol{K}}{2}[\boldsymbol{ln}(\boldsymbol{J})]^2 \quad (1)$$

Here, $\tilde{I}_1$ and $\tilde{I}_2$ are the first and second invariants of the deviatoric version of the right Cauchy–Green deformation tensor, respectively. $\tilde{\lambda}$ is the deviatoric part of the stretch along the fibre direction, and $J = det(F)$ is the Jacobian of the deformation. This strain energy density function consists of two parts: F_1 represents the material response of the isotropic ground substance matrix, while F_2 represents the contribution from the collagen fibres. F_1 was described as a Neo-Hookean model and was equal to $\frac{C_1(I_1-3)}{2}$. The resulting fibre stress from the fibres was expressed using the following piecewise function *(2)*:

	SOL force (N)	GM force (N)	GL force (N)
BiRise	827.6 ± 184.4	205.5 ± 37.9	91.0 ± 18.5
BiDrop	847.7 ± 178.6	246.6 ± 71.7	117.6 ± 28.8
UniDrop	1852.7 ± 671.3	439.7 ± 119.4	149.7 ± 35.2
Walk	1603.6 ± 402.8	627.4 ± 219.9	187.7 ± 63.4
UniDrop Bent	2324.4 ± 636.9	430.1 ± 141.2	145.5 ± 80.6
BiHop	3565.2 ± 680.8	416.6 ± 270.5	82.02 ± 100.5

Table 2. The table presents the generic muscle force values for six rehabilitation exercises, used as boundary conditions for loading the three sub-tendons (SOL, GM, and GL) of the FE models. These generic muscle forces were determined by averaging subject-specific muscle forces from the triceps surae muscles across 21 participants across the six rehabilitation exercises (in the table: mean ± SD, measured in Newtons (N)).

Content courtesy of Springer Nature, terms of use apply. Rights reserved



	Subject-specific model	Material model	Muscle forces model
Geometry	subject-specific	subject-specific	subject-specific
Elastic modulus	subject-specific	subject-specific	average
Muscle forces	subject-specific	average	subject-specific

Fig. 1. Overview of the features of the FE models. On the top, anterior and posterior view of an example of Achilles free tendon geometry, representing the least twisted geometry described by Pękala et al.[18]. The figure displays an AT model from the left limb. The 3D tendon models were divided into three sub-tendons, each arising from one of the three triceps surae muscles: the soleus (SOL) and the two heads (medialis, GM and lateralis, GL) of the gastrocnemius muscle. On the bottom, a summary of the characteristics of the three different models.

$$\tilde{\lambda}\,\frac{\partial \boldsymbol{F}_2}{\partial\,\tilde{\lambda}} = \begin{cases} 0 & \tilde{\lambda} \le 1 \\ \boldsymbol{C}_3\left(\boldsymbol{e}^{\boldsymbol{C}_4\left(\tilde{\lambda}-1\right)}-1\right) & 1 < \tilde{\lambda} < \lambda_m \\ \boldsymbol{C}_5\,\tilde{\lambda} + \boldsymbol{C}_6 & \tilde{\lambda} \ge \lambda_m \end{cases} \tag{2}$$

Here, λ_m is the stretch at which the fibres are straightened, C_3 is the scaling of the exponential stress, C_4 is the rate of uncrimping of the fibres and C_5 is the Young's modulus of the straightened fibres. C_6 is determined from the requirement that the stress is continuous at λ_m. For the *subject-specific model* and *material model*, each participant had a different C_5 value, which was calculated using the subject-specific stress–strain curve as described above. For the *muscle forces model*, the C_5 value was the average of the subject-specific E values (Table 1). The values of the other material coefficients (C_1, C_3, and C_4) were not subject-specific and were obtained from Shim et al.[24], which involved tendinopathic tendons. After conducting a sensitivity analysis to assess the influence of material coefficients on the output of the FE models, it was considered appropriate to estimate only the subject-specific C_5, considering the available experimental data. The constitutive models implemented in FEBio Studio[34] as "*trans iso Mooney-Rivlin*" were used in this study. The sub-tendons fascicles were modelled using FEBio's local fibre direction function (a_0)[34], which was defined for each element to represent the tendon fascicle structure[35]. For each sub-tendons, fibres were directed from the proximal cross-section to the distal cross-section. In this way, the resulting local fibres could follow the twisting structure of the sub-tendons.

Creation of FE models with subject-specific geometry with free-form deformation

Subject-specific FE models were generated using subject-specific geometry. First, 2D ultrasound images of the tendon under resting conditions were transformed into a global coordinate system using 3D Slicer software to create a reconstructed 3D volume. After computing a 3D volume reconstruction, the AT was manually outlined using the reconstructed 2D images, and the corresponding borders were combined to generate 3D data clouds

Content courtesy of Springer Nature, terms of use apply. Rights reserved

that captured the tendon geometry. In total, 21 subject-specific 3D shapes were obtained. Subsequently, the template mesh containing three sub-tendons was customized to each subject-specific geometry obtained from the participant's 3DfUS image. The free-form deformation method[36] was used, which morphs an underlying mesh by embedding it inside a host mesh. The external and internal nodes of a given mesh are deformed with the same transformation to match the subject's geometry. In this way, it was possible to obtain subject-specific free AT geometries for each participant, representing the least twisting structure described in the literature[18].

FE models boundary conditions

The models boundary conditions were defined in FEBio[34]. The contact between the three sub-tendons was defined as frictionless sliding[35]. The distal end of the tendon models was fixed to mimic the attachment of the tendon to the calcaneus. The muscle forces for the different rehabilitation exercises were applied as nodal loads to the proximal faces of each sub-tendon. The nodal displacements were constrained to move only in the distal-proximal direction to mimic the constraints provided by the paratenon and fascia cruris that hold the sub-tendons together[37].

Internal tissue strain analysis

Analyses were conducted to quantitatively examine the strain distribution patterns during various exercises in the FE models. The average of the maximum principal strain in the mid-portion (defined as the middle third of the AT models) of the *subject-specific models* was analysed to rank the rehabilitation exercises for the 21 participants (Fig. 2). The ranking of the exercises is based on the mean of the average strains among all the participants. An optimal strain range was used between 5% and 7% tendon strain based on Pizzolato et al.[38] while allowing for a margin of error of up to 1% strain. The mid-portion of the subject-specific tendon models was chosen for strain analysis because the study involved patients with mid-portion Achilles tendinopathy. This area is particularly impacted by pathological changes[39], making it crucial to investigate the strains here to determine if the tendon undergoes positive adaptation and tissue recovery is promoted. Second, we investigated the distribution of the maximum principal strain and identified the location and magnitude of the peak maximum principal strain across the *subject-specific models*. This was done to characterize the overall strain patterns associated with

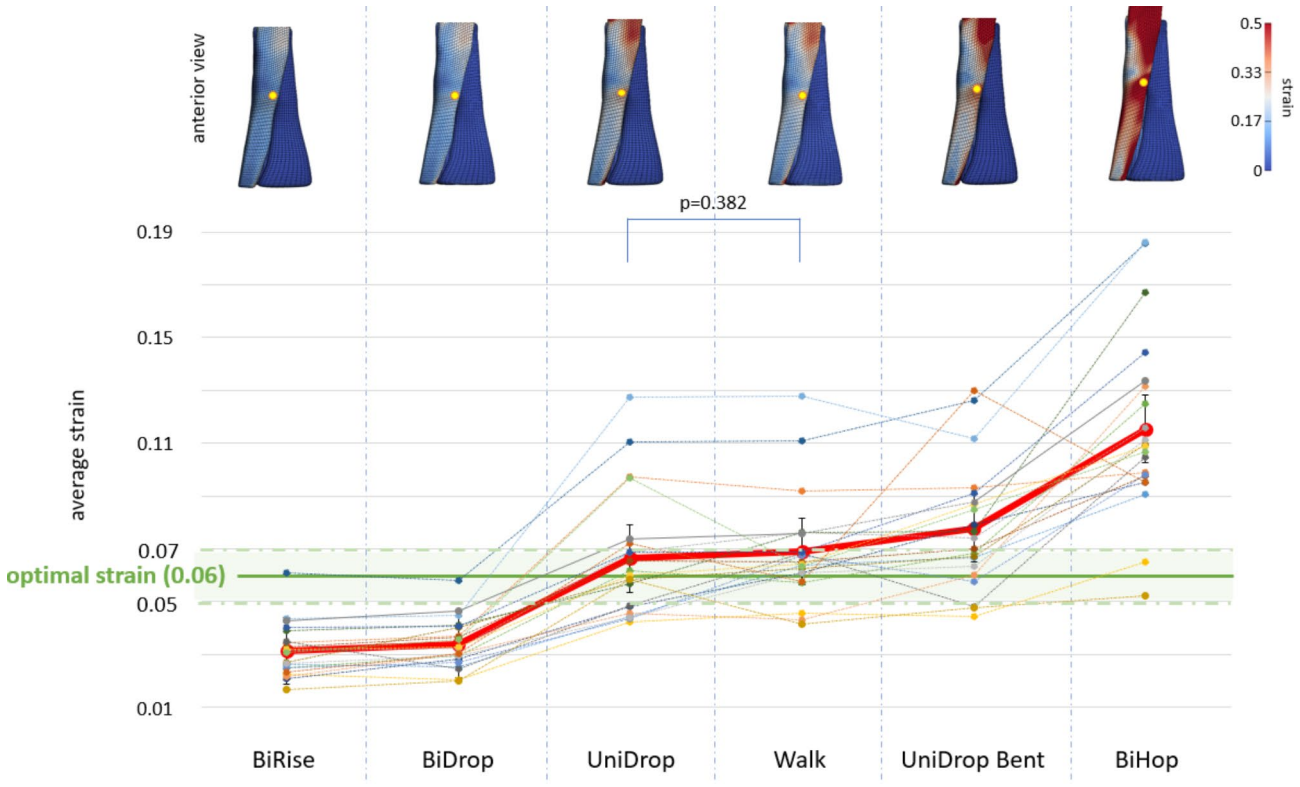


Fig. 2. Strain distribution and generalized and individual rankings of the rehabilitation exercises. On the top, a representative example of the distribution of the maximum principal strain within the entire free AT model for each exercise from one participant. The yellow dots indicate the location of the peak strain. On the bottom, the red line represents the mean of the average strain during each exercise in the mid-portion of the subject-specific models. Exercises are ranked based on this average strain. The dotted lines represent the average strain during the exercises for each participant in the mid-portion of the subject-specific models. The optimal strain, designated 0.06 (6%) according to Pizzolato et al.[38], is represented by the green bar, which highlights the range defined as 0.06 ± 0.01 ($6 \pm 1\%$) strain. All exercises showed statistically significant differences except for the unidrop and walk exercises. The significance level was set at $p < 0.05$.

Content courtesy of Springer Nature, terms of use apply. Rights reserved

different exercises (Fig. 2). The peak strain location was determined across the entire free tendon, excluding the regions where load boundary conditions were applied, in line with Saint-Venant's principle. The average and peak of the maximum principal strain in the mid-portion of the *material models* and *muscle forces models* were analysed for subsequent regression analysis.

Statistical analysis

Statistical analysis of the strains in the mid-portion of the AT models was performed using SPSS Statistics software (IBM Corp. (2017)). IBM SPSS Statistics for Windows (Version 29.0.1.0). Armonk, NY: IBM Corp.). Repeated measures ANOVA was performed to compare the means of the average and peak strains in the mid-portion of the *subject-specific models* across the exercises. If a significant main effect was found, the least significant difference (LSD) for post hoc testing was applied to identify the exercises whose means were significantly different. All the data are presented as mean ± SD. The statistical level of significance was set as $p < 0.05$. In the subsequent analysis, linear regression was conducted to assess the impact of subject-specific material properties and subject-specific muscle forces on the average and peak strains in the mid-portion of the AT FE models. For significant correlations, the coefficients of correlation (r) between the *subject-specific model* and *material model* and between the *subject-specific model* and *muscle forces model* were compared.

Results

Subject-specific models

Ranking of the Rehabilitation exercises based on Tendon strains

Starting from the lowest average strain in the mid-portion of the *subject-specific models*, the generalized ranking of rehabilitation exercises was as follows: birise (0.031 ± 0.010), bidrop (0.034 ± 0.009), unidrop (0.066 ± 0.023), walk (0.069 ± 0.020), unidrop bent (0.078 ± 0.023), and bihop (0.115 ± 0.033). All exercises demonstrated statistically significant differences from one another, except for unidrop and walk, as depicted in Fig. 2. Notably, at peak total muscle force, only unidrop and walk showed average strains within the range of the reported optimal strain when the generalized ranking was evaluated. However, when evaluated at the individual level, the variations in average strain across participants become more evident not only in the exercise rankings but also in the exercises that fall within the optimal strain range. This indicates that participants achieved optimal strain levels during different exercises. While the majority of participants reached optimal strain levels during the unidrop and walk exercises (eight and 12 participants, respectively), individual rankings revealed that the optimal strain range could also be obtained during the unidrop bent exercise for seven participants, the bihop for two participants, the birise for one participant, and the bidrop for one participant (Fig. 2).

Strain distribution, peak location and peak strain values

The peak strain consistently occurred in the middle of the mid-portion or upper mid-portion, at the edge of the SOL sub-tendon, which is the sub-tendon exposed to the highest muscle forces (Table 2). However, there was marked variability in the exact location of the peak strain and strain distribution among participants, as illustrated in Fig. 3. Conversely, within a participant, both the peak location and strain distribution remained consistent throughout the exercises (as shown in Fig. 2). Nevertheless, the magnitude of peak strain varied depending on the load applied during each exercise. The peak strain values in the mid-portion of the subject-specific models were as follows: birise, 0.194 ± 0.081; bidrop, 0.196 ± 0.069; unidrop, 0.481 ± 0.299; walk, 0.403 ± 0.209; unidrop bent, 0.648 ± 0.389; and bihop, 0.963 ± 0.462. All the exercises exhibited significant differences ($p < 0.05$) from each other, except for birise and bidrop ($p = 0.774$) and walk and unidrop ($p = 0.061$).

Material models and muscle forces models

Regression analysis

Scatterplots depicting the average and peak of the maximum principal strain in the mid-portion of the AT models for the *material models* and the *muscle forces models* are presented in Fig. 4. The association between the *subject-specific model* and the *material model* yielded a lower r than did the association between the *subject-specific model* and *muscle forces model*. For the *material model*, the RMSE values were found to be 0.016 and 0.223, for average and peak strain, respectively. For the *muscle forces model*, the RMSE values were 0.006 and 0.151, for the average and peak strain, respectively. The RMSE values indicate a good fit of the *subject-specific model* to both the *material* and *muscle forces model*. However, a greater similarity in strain magnitude between the *muscle forces model* and the *subject-specific model* is observable in Fig. 5, which indicates that the influence of the subject-specific *E* has a lesser impact on the strains of the *subject-specific model* than does the influence of subject-specific muscle forces.

Discussion

The primary objective of this research was to assess tendon strains during various rehabilitation exercises in patients with Achilles tendinopathy, with the aim of ranking the exercises based on average strain in the mid-portion of the AT. We utilized FE models that incorporated several patient-specific features, including the AT outer geometry, the Elastic modulus of the tendon fibres, and the muscle forces generated during rehabilitation exercises. Applying these models provided us with novel insights: despite participants performing the same exercise, they exhibited varying strains in the mid-portion of their AT. Furthermore, these models highlighted that the variability in tendon strains primarily stemmed from differences in muscle forces rather than material properties. This study successfully determined a ranking of the rehabilitation exercises aimed at gradually increasing the strains in the mid-portion of the AT. The recommended progression begins with concentric and eccentric exercises, such as bilateral heel rise, bilateral heel drop and unilateral heel drop, and advances to more

Content courtesy of Springer Nature, terms of use apply. Rights reserved

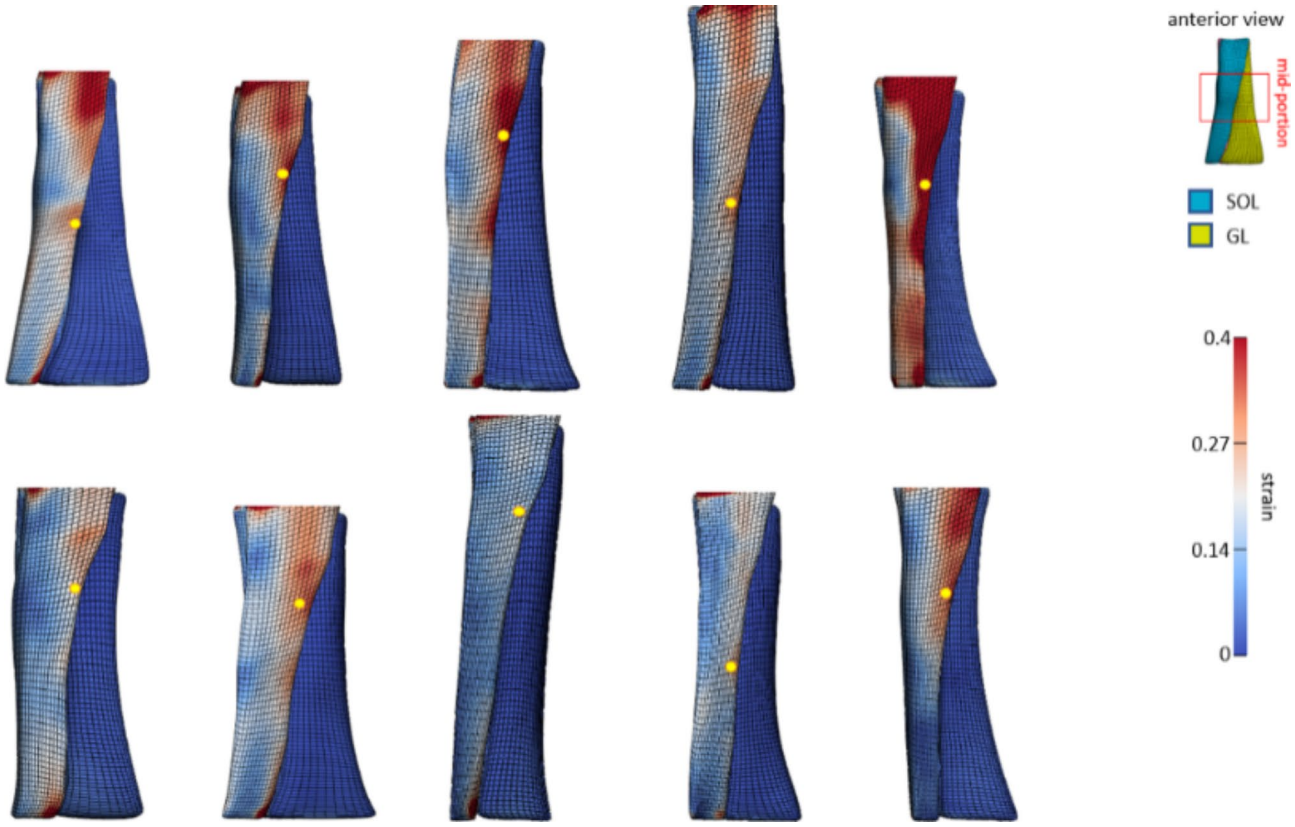


Fig. 3. Representative examples of the maximum principal strain distribution across the entire free AT models for 10 participants during walking. The anterior view of the subject-specific models is presented, highlighting the SOL sub-tendon with the highest strains. The yellow dots indicate peak strains, which are predominantly located in the middle and upper parts of the mid-portion of the SOL sub-tendon. The mid-portion refers to the middle third of the model, which has been highlighted within the full free AT model, as shown in the top right corner of the figure. The peak strain location is determined across the entire free tendon, excluding the regions where boundary conditions were applied in accordance with Saint-Venant's principle; these regions are not depicted in the figure.

functional exercises, such as walking, unilateral heel drop with flexed knee and bilateral hopping. There was no significant difference between the unilateral heel drop and walking exercise, and the values fell within the optimal strain range. However, when analysing individual strains, there was variability in exercise rankings among participants, as well as exercises falling within the optimal strain range. Last, variability between participants in terms of strain was more closely related to subject-specific muscle forces than to material properties.

Ranking of the rehabilitation exercises based on tendon strains

In accordance with our hypothesis, the resulting generalized ranking delineated a sequence of rehabilitation exercises to gradually increase tendon strains, starting with the relatively low-load concentric bilateral heel rise and progressing towards the eccentric bilateral heel drop. While Alfredson et al.[6] recommended incorporating unilateral heel drop exercise during the initial phase, Silbernagel et al.[7] suggested it be introduced in a later stage of the rehabilitation program due to concerns about tendon overload. Our results demonstrated that unilateral heel drop induced greater strain in the AT than did the two bilateral exercises. However, this increased load caused by the unilateral heel drop achieves optimal strain levels[10], which suggests that this approach can be used in the initial phase of the rehabilitation program. Similar to other studies[25,40], we confirmed that walking also falls within the optimal strain range necessary for AT tissue healing, although walking exposes the AT to a load approximately four times the body weight[41]. This suggests that patients with Achilles tendinopathy may safely engage in walking activities as part of their rehabilitation program from the beginning without significant disruption to their daily routines.

In adherence to Alfredson's protocol[6], we also incorporated a unilateral heel drop with flexed knee exercise. This exercise plays a pivotal role in the rehabilitation program by enhancing the activation of the soleus muscle and facilitating a redistribution of muscle forces. However, the increased activation of the soleus led to increased strains, which surpassed the optimal range. It is known that the AT experiences high loads during hopping, equivalent to approximately five times body weight[41]. Indeed, our simulation of hopping exercises reflected these high loads, resulting in strains surpassing the optimal threshold. Nevertheless, our calculations of tendon strains during hopping surpassed those reported in earlier research[25]. For example, Lichtwark et al.[42] noted a

Content courtesy of Springer Nature, terms of use apply. Rights reserved

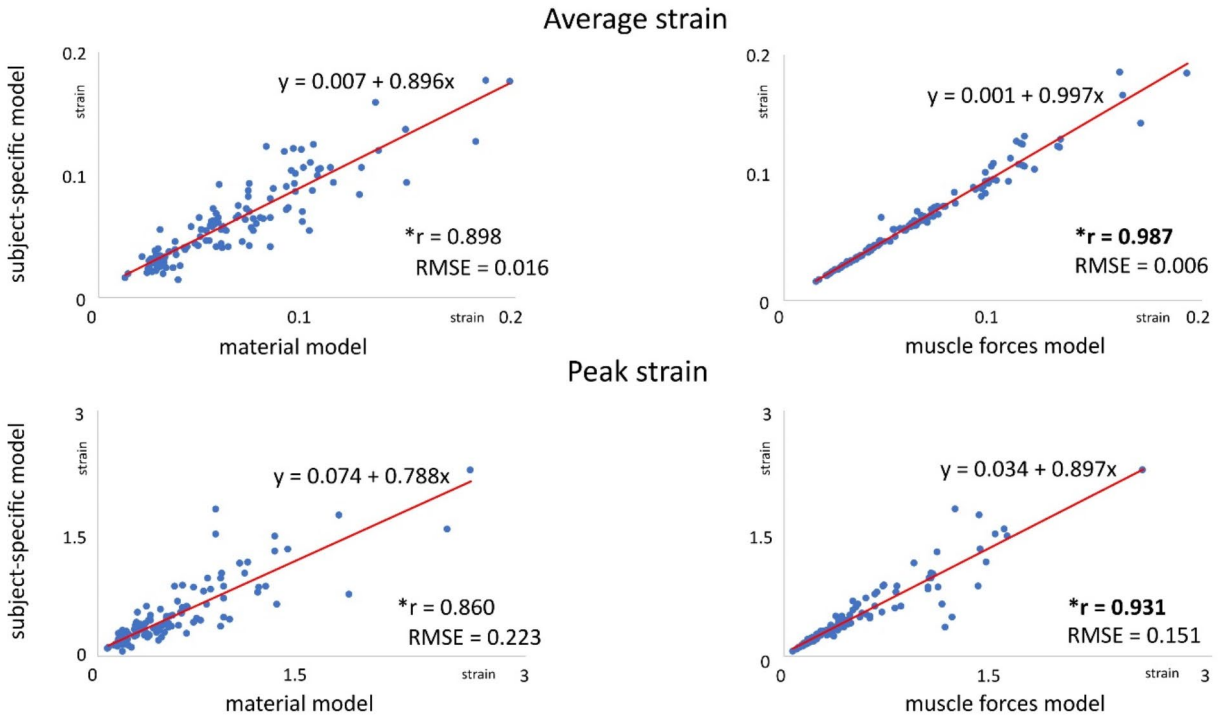


Fig. 4. Scatterplots and linear regression lines of comparisons of the *subject-specific model* with the *material model* and *muscle forces model* for the average (on the top) and peak (on the bottom) strains in the mid-portion of the AT models. The coefficient of correlation (r) computed across all the participants and exercises is also displayed in each plot. The * indicates statistical significance ($p < 0.05$). The plot also includes the regression equation, which illustrates the relationship between the variables, as well as the root mean square error (RMSE).

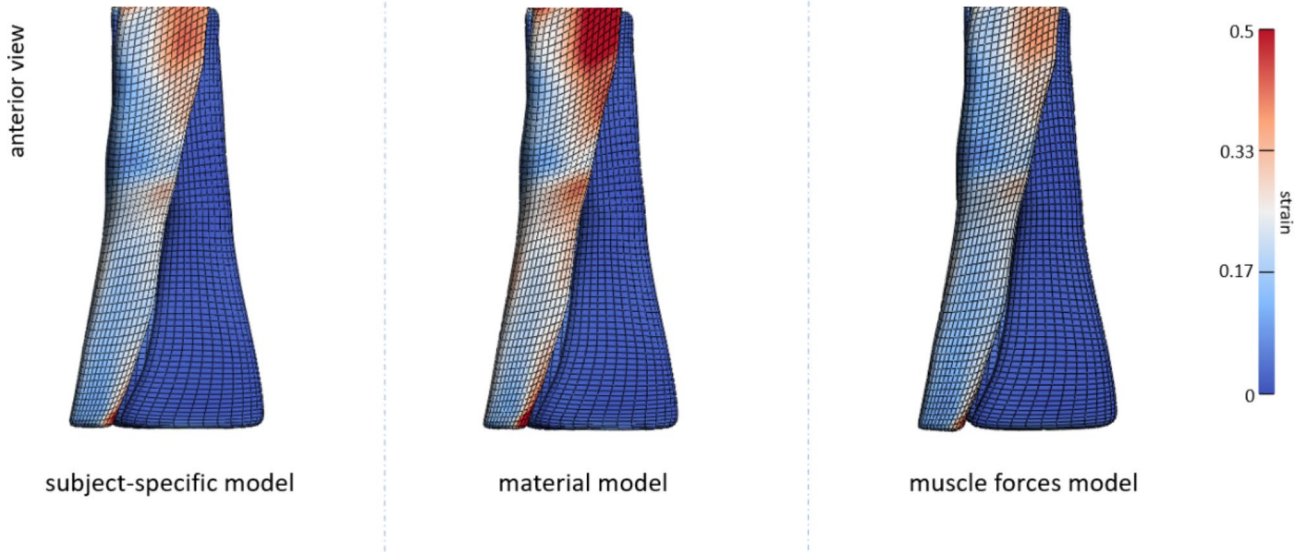


Fig. 5. Representative examples of the strain distribution for the three types of AT models developed: *subject-specific model, material model and muscle forces model*. An example is presented for one participant during the simulation of walking. The examples represent the entire free AT, excluding strain data at the top boundary of the model, in accordance with Saint-Venant's principle. While the strain distribution and peak strain location remain constant among the models, the image shows a high correlation of the strain magnitude between the *subject-specific model* and the *muscle forces model*, as demonstrated by the high r value.

Content courtesy of Springer Nature, terms of use apply. Rights reserved

peak strain of 8.3% during unilateral hopping, with tendon strains measured at the gastrocnemius medialis myotendinous junction level. The probable explanation for these discrepancies lies in the fact that our strain assessments were based on free AT, which undergoes notably greater longitudinal strain than aponeurosis[43,44]. Also, our study includes patients with Achilles tendinopathy, who typically have more compliant tendons[15]. As a result, they may develop higher strains compared to those observed in studies involving healthy subjects. Moreover, the strains that we reported are from computational models, where the strains are measured at the element level. This includes some localized peak strains that are not captured by the global strains measured in the abovementioned studies. This might have also caused the greater number of strains that we observed in our study. Finally, the definition of the optimal strain levels requires careful interpretation. Both underloading and overloading are detrimental to the AT, and a specific strain threshold must be reached to promote positive tendon adaptation. As a threshold for optimal strain levels, we used the value from Pizzolato et al.[38] (approximately 6%). This value is based on both in-vivo human study[11] and in-vitro animal study[10], conducted on healthy tendons, and it represents the only available data. Further research is needed to clarify the specific loading conditions (e.g., magnitude, duration, frequency, and rate) that maximize tendon adaptation, especially in tendinopathic tendons.

Our simulations were based on FE models developed for patients at the beginning of their rehabilitation program. Considering the likelihood of morphological and material property alterations throughout the rehabilitation process, it becomes pertinent to explore how these modifications could impact AT strains. This analysis could inform the right timing of activities such as unilateral heel drop with flexed knee and hopping within the rehabilitation program. For instance, Silbernagel et al.[45] suggested incorporating such activities in a later stage with the return-to-sport program. By evaluating the rehabilitation stages and monitoring strain variations together with morphological and material properties changes, we can ensure that patients with Achilles tendinopathy undergo a phased and carefully managed recovery process by appropriate loading of the AT. Furthermore, with additional data, these FE models could potentially identify tendon characteristics, including morphological features, that indicate the strain status and predict the specific exercise to promote positive adaptation. These morphological features can be quantified using ultrasound imaging, which is readily accessible to physiotherapists in clinical practice. This capability could assist physiotherapists in making informed decisions when prescribing rehabilitation exercises tailored to the biomechanical condition of the tendon.

The unique characteristics of the subject-specific responses were evident when inspecting the tendon strains of the individual patients with Achilles tendinopathy. Based on our results, it becomes clear that a generic approach is insufficient since variations in tendon strains among participants for a specific rehabilitation exercise become visible. While unilateral heel drop and walking were the most common exercises among participants (eight and 12 participants, respectively), optimal strains were observed in seven participants during unilateral heel drop with a flexed knee, supporting the theory of eccentric exercises as the preferred treatment for patients with Achilles tendinopathy[6]. Interestingly, bilateral heel rise and bilateral heel drop exercises consistently resulted in suboptimal strain levels across individual rankings, with only one participant achieving the optimal strain for both exercises. Further exploration of these cases could provide further insights into what characteristics determine these individual tendon strains.

Notably, the participant who achieved optimal strain during bilateral heel rise and bilateral heel drop exhibited an E comparable to the average (709.1 vs. 631.9 MPa, individual and average E, respectively), suggesting that material properties alone may not be decisive in this case. Indeed, anthropometric analysis revealed that this participant had a greater weight compared to the average (80 vs. 76 kg, individual and average weight, respectively) and greater muscle forces during the execution of these exercises. Furthermore, analysis of AT morphology highlighted a significantly smaller CSA (the smallest CSA, more specifically) in the mid-portion of the AT model among the participants (66.4 vs. 112.3 mm^2, individual and average CSA, respectively). The combination of these factors led to greater strains during the performance of two generally low-load exercises and thus the achievement of the optimal strains earlier during the progression of the rehabilitation exercises. Therefore, the necessity of personalized exercise prescriptions tailored to individual muscle forces and tendon morphology becomes evident since the strains seem to be highly dependent.

Bilateral hopping was the exercise imposing the highest load on the AT for all participants and, for this reason, was generally located at the end of the rehabilitation exercise progression, given the high strains produced. Nevertheless, for two participants, this exercise led to optimal strains. Again, individual characteristics such as the material and morphological properties of the AT and muscle forces offer insights into this variation. The E and CSA of one of these two participants were similar to those of other participants (498.2 vs. 478.5 MPa and 111.8 vs. 99.8 mm^2, respectively, for the first and second participants). However, while one of the participants only reached the optimal strain level later in the exercise progression, during bilateral hopping, the other achieved it during walking, demonstrating consistently greater strains compared to the former. This difference is coming from the force production: the second participant generated greater strains due to greater muscle forces. This closer analysis also demonstrated that when evaluating strains, it is crucial to consider all subject-specific characteristics. In this case, neglecting subject-specific muscle forces could have introduced errors into the analysis.

These two examples highlight the significant sensitivity of AT strains to the individual muscle forces and geometry of each subject. This sensitivity is further supported by the findings of the regression analysis. According to our hypothesis, our investigation established that the strains were more closely related to the subject-specific muscle forces than to the material properties. In line with previous results[22,24], it becomes evident that when creating subject-specific models, prioritizing not only subject-specific geometry but also subject-specific muscle forces over material properties is crucial for a more accurate representation of AT strains, especially when considering patients with Achilles tendinopathy. Mylle et al.[19] demonstrated a different force distribution strategy between patients with Achilles tendinopathy and healthy controls. This altered strategy at the triceps

Content courtesy of Springer Nature, terms of use apply. Rights reserved

surae muscles determines altered force transmission to the AT, influencing AT loading and, consequently, AT strains. These outcomes underscore the complex nature of individual AT responses to load, emphasizing the importance of tailoring rehabilitation protocols to subject-specific characteristics, especially geometry and muscle forces. Nonetheless, the definition of an average ranking of rehabilitation exercises contributes to a general understanding of the diverse effects these exercises have on AT strains at the population level.

Strain distribution, peak location and peak strain values

Using subject-specific FE models for a large patient population demonstrated that strain distribution and peak strain location are influenced more by geometry than muscle forces. Regardless of the type of exercise, the peak strain was consistently observed in the middle or upper mid-portion of the edge of the SOL sub-tendon, which is the most loaded sub-tendon. This finding aligns with findings indicating that tendinopathic tendons exhibit non-uniform tendon longitudinal morphology strain along their length under load, with the mid-portion undergoing larger strains[46]. Furthermore, the mid-portion is the location of the most pronounced pathological changes in tendon structure and composition in patients with Achilles tendinopathy. Consequently, these changes in tendon thickness, fibre alignment, and collagen distribution can influence the mechanical behaviour of the tendon. The location of the peak strain in the mid-portion can also be explained by the fact that the least twisted geometry (corresponding to Type I twist described by Pękala et al.[18]) was represented in this study. We decided to develop only this twisting geometry because it is the most common among individuals[18], and in our previous study, we demonstrated that the average strain in the mid-portion of the AT is not affected by the type of twist[20]. However, the twist influences the location of the peak strain, with Type I exhibiting the highest strain in the mid-portion of the tendon for some exercises. Moreover, the peak strain was consistently observed at the edge of the SOL sub-tendon. This finding aligns with previous observations[21,35,47,48], where the highest strain and stress were located at the edges of the sub-tendons. At this location, differences in sliding between the sub-tendons, due to the differential application of muscle forces, can lead to the development of interface strains[47]. Although the peak strain consistently occurred in the mid-portion of the AT models, there was significant variability in the exact location of the peak among participants, as illustrated in Fig. 3. These variations could be influenced by various factors, including the location of the swelling caused by tendinopathy or other attributes of the tendon's geometry, including its shape, width, and length. Understanding this information could aid in predicting the likelihood of experiencing the highest strain in specific areas of the tendon for patients with Achilles tendinopathy. This insight may also contribute to strategies for preventing or treating this condition. Therefore, additional research is necessary.

Limitations

This study has also some limitations, which will be discussed in this section. The frictional contact between sub-tendons to account for the compromised sliding mechanism, which leads to more uniform deformations in the AT of patients with Achilles tendinopathy[49], was not used in our current FE model. It was not deemed essential to incorporate this feature into our current model to address our research questions. However, the future development of FE models of patients with Achilles tendinopathy will necessitate the incorporation of subject-specific frictional contact to also consider alterations in non-uniform deformation within sub-tendons for the estimation of AT strains. In general, positive AT adaptation is not only dependent on strain magnitude but also time- and rate-dependent[10,50]. However, the loading rate is a factor not accounted for in our model, given the decision to use a hyperelastic material as a constitutive model for AT. The choice of hyperelastic material aligns with common practices in FE models of the AT[22,24,35,51], assuming that tendons are in a 'preconditioned state'[33]. Given the application of load for a specific time point (time of peak total muscle force) during the execution of the exercise, the incorporation of a viscoelastic material was considered noncrucial. The subsequent development of FE AT models could explore the integration of viscoelastic material properties to assess the impact of the loading rate on AT strains. Moreover, while our study focused on the tensile loads and tensile strains of the AT, it is important to note that the mid-portion of the AT may also experience compressive loads[52]. However, as the rehabilitation exercises primarily involve tensile loading, we believed that it was reasonable to neglect the compressive load component in our current analysis. Further investigations with FE AT models could investigate compressive loads to provide a comprehensive understanding of AT strains during rehabilitation exercises. Furthermore, although the strains predicted by these FE models align with values reported in previous literature, future studies need to validate these models against controlled experimental data. This would ensure even greater precision in predicting tendon strain patterns under various rehabilitation protocols. Finally, future studies should integrate these strain estimations into rehabilitation protocols to assess whether a program enables patients to achieve these targeted strain values, facilitating positive tendon adaptation tailored to individual patient characteristics.

Conclusions

In conclusion, we provided a ranking of various rehabilitation exercises for patients with Achilles tendinopathy based on the average strain in the mid-portion of the AT models. The analysis of individual rankings revealed noticeable variations in strain distribution patterns among participants. This finding highlights the importance of tailored rehabilitation protocols that consider individual patient-specific morphological and material characteristics and muscle forces. Furthermore, subject-specific FE models proved to be a valuable tool for explaining the relationship between rehabilitation exercises and tendon strains. Our study highlights the significance of prioritizing not only subject-specific geometry but also subject-specific muscle forces when creating FE models aimed at estimating the AT strain in patients with Achilles tendinopathy. While further research is needed to validate the presented in silico approach, the outcomes of this study provide a significant initial contribution to the future development of biomechanically informed rehabilitation protocols.

Content courtesy of Springer Nature, terms of use apply. Rights reserved

Data availability

The source data are available to verified researchers upon request by contacting the corresponding author.

Received: 11 December 2024; Accepted: 20 December 2024
Published online: 07 January 2025

References

1. Maffulli, N. & Kader, D. Tendinopathy of tendo Achillis. *J. Bone Jt. Surg. Ser. B* **84**, 1–8 (2002).
2. Sleeswijk Visser, T. S. O. et al. Impact of chronic Achilles tendinopathy on health-related quality of life, work performance, healthcare utilisation and costs. *BMJ Open Sport Exerc. Med.* **7**, 1–7 (2021).
3. Rolf, C. & Movin, T. Etiology, histopathology, and outcome of surgery in achillodynia. *Foot Ankle Int.* **18**, 565–569 (1997).
4. Maffulli, N., Sharma, P. & Luscombe, K. L. Achilles tendinopathy: aetiology and management. *J. R. Soc. Med.* **97**, 472–476 (2004).
5. Cook, J. L. & Purdam, C. R. The challenge of managing tendinopathy in competing athletes. *Br. J. Sports Med.* **48**, 506–509 (2014).
6. Alfredson, H., Pietilä, T., Jonsson, P. & Lorentzon, R. Heavy-load eccentric calf muscle training for the treatment of chronic achilles tendinosis. *Am. J. Sports Med.* **26**, 360–366 (1998).
7. Silbernagel, K. G., Thomeé, R., Thomeé, P. & Karlsson, J. Eccentric overload training for patients with chronic Achilles tendon pain - A randomised controlled study with reliability testing of the evaluation methods. *Scand. J. Med. Sci. Sport.* **11**, 197–206 (2001).
8. Mascaró, A. et al. Load management in tendinopathy: Clinical progression for Achilles and patellar tendinopathy. *Apunt. Med. l'Esport* **53**, 19–27 (2018).
9. Malliaras, P., Barton, C. J., Reeves, N. D. & Langberg, H. Achilles and patellar tendinopathy loading programmes: A systematic review comparing clinical outcomes and identifying potential mechanisms for effectiveness. *Sport. Med.* **43**, 267–286 (2013).
10. Wang, T. et al. Cyclic mechanical stimulation rescues achilles tendon from degeneration in a bioreactor system. *J. Orthop. Res.* **33**, 1888–1896 (2015).
11. Arampatzis, A., Karamanidis, K. & Albracht, K. Adaptational responses of the human Achilles tendon by modulation of the applied cyclic strain magnitude. *J. Exp. Biol.* **210**, 2743–2753 (2007).
12. Maffulli, N., Walley, G., Sayana, M. K., Longo, U. G. & Denaro, V. Eccentric calf muscle training in athletic patients with Achilles tendinopathy. *Disabil. Rehabil.* **30**, 1677–1684 (2008).
13. De Mos, M. et al. Achilles tendinosis: Changes in biochemical composition and collagen turnover rate. *Am. J. Sports Med.* **35**, 1549–1556 (2007).
14. Wang, J. H. C. Mechanobiology of tendon. *J. Biomech.* **39**, 1563–1582 (2006).
15. Arya, S. & Kulig, K. Tendinopathy alters mechanical and material properties of the Achilles tendon. *J. Appl. Physiol.* **108**, 670–675 (2010).
16. Shim, V. B., Handsfield, G. G., Fernandez, J. W., Lloyd, D. G. & Besier, T. F. Combining in silico and in vitro experiments to characterize the role of fascicle twist in the Achilles tendon. *Sci. Rep.* **8**, 1–12 (2018).
17. Edama, M. et al. The twisted structure of the human Achilles tendon. *Scand. J. Med. Sci. Sport.* **25**, e497–e503 (2015).
18. Pękala, P. A. et al. The twisted structure of the Achilles tendon unraveled: A detailed quantitative and qualitative anatomical investigation. *Scand. J. Med. Sci. Sports* **27**(12), 1705–1715 (2017).
19. Mylle, I., Crouzier, M., Hollville, E., Bogaerts, S. & Vanwanseele, B. Triceps surae muscle forces during dynamic exercises in patients with Achilles tendinopathy: A cross-sectional study. *Scand. J. Med. Sci. Sports* **33**(11), 2219–2229. https://doi.org/10.1111/sms.14444 (2023).
20. Funaro, A., Shim, V., Crouzier, M., Mylle, I. & Vanwanseele, B. Subject-specific 3D models to investigate the influence of rehabilitation exercises and the twisted structure on Achilles tendon strains. *Front. Bioeng. Biotechnol.* **10**, 1–9 (2022).
21. Yin, N.-H., Fromme, P., McCarthy, I. & Birch, H. L. Individual variation in Achilles tendon morphology and geometry changes susceptibility to injury. *Elife* **10**, e63204 (2021).
22. Hansen, W. et al. Achilles tendon stress is more sensitive to subject-specific geometry than subject-specific material properties: A finite element analysis. *J. Biomech.* **56**, 26–31 (2017).
23. Shim, V. B. et al. Subject-specific finite element analysis to characterize the influence of geometry and material properties in Achilles tendon rupture. *J. Biomech.* **47**, 3598–3604 (2014).
24. Shim, V. B. et al. Influence of altered geometry and material properties on tissue stress distribution under load in tendinopathic Achilles tendons – A subject-specific finite element analysis. *J. Biomech.* **82**, 142–148 (2019).
25. Devaprakash, D. et al. Free Achilles tendon strain during selected rehabilitation, locomotor, jumping, and landing tasks. *J. Appl. Physiol.*
26. Craig, C. L. et al. International physical activity questionnaire: 12-Country reliability and validity. *Med. Sci. Sports Exerc.* **35**, 1381–1395 (2003).
27. Merza, E., Pearson, S., Lichtwark, G., Garofolini, A. & Malliaras, P. Reliability of human Achilles tendon stiffness measures using freehand 3-D ultrasound. *Ultrasound Med. Biol.* **47**, 973–981 (2021).
28. Maganaris, C. N., Baltzopoulos, V. & Sargeant, A. J. Changes in Achilles tendon moment arm from rest to maximum isometric plantarflexion: In vivo observations in man. *J. Physiol.* **510**, 977–985 (1998).
29. Raiteri, B. J., Cresswell, A. G. & Lichtwark, G. A. Ultrasound reveals negligible cocontraction during isometric plantar flexion and dorsiflexion despite the presence of antagonist electromyographic activity. *J. Appl. Physiol.* **118**, 1193–1199 (2015).
30. Delp, S. L. et al. An interactive graphics-based model of the lower extremity to study orthopaedic surgical procedures. *IEEE Trans. Biomed. Eng.* **37**, 757–767 (1990).
31. De Groote, F., De Laet, T., Jonkers, I. & De Schutter, J. Kalman smoothing improves the estimation of joint kinematics and kinetics in marker-based human gait analysis. *J. Biomech.* **41**, 3390–3398 (2008).
32. De Groote, F., Kinney, A. L., Rao, A. V. & Fregly, B. J. Evaluation of direct collocation optimal control problem formulations for solving the muscle redundancy problem. *Ann. Biomed. Eng.* **44**, 2922–2936 (2016).
33. Weiss, J. A., Maker, B. N. & Govindjee, S. Finite element implementation of incompressible, transversely isotropic hyperelasticity. *Comput. Methods Appl. Mech. Eng.* **135**, 107–128 (1996).
34. Maas, S. A., Ellis, B. J., Ateshian, G. A. & Weiss, J. A. FEBio: Finite elements for biomechanics. *J. Biomech. Eng.* **134**, (2012).
35. Knaus, K. R. & Blemker, S. S. 3D models reveal the influence of achilles subtendon twist on strain and energy storage. *Front. Bioeng. Biotechnol.* **9**, 1–10 (2021).
36. Fernandez, J. et al. Musculoskeletal modelling and the physiome project. In *Multiscale Mechanobiology of Bone Remodeling and Adaptation* (ed. Pivonka, P.) 123–174. https://doi.org/10.1007/978-3-319-58845-2_3 (Springer International Publishing, 2018).
37. Diniz, P. *et al.* Design and validation of a finite element model of the aponeurotic and free Achilles tendon. *J. Orthop. Res.* 41: 534–545 (2022) https://doi.org/10.1002/jor.25408.
38. Pizzolato, C. et al. Finding the sweet spot via personalised Achilles tendon training: The future is within reach. *Br. J. Sports Med.* **53**, 11–12 (2019).
39. Gervasio, A., Bollani, P. & Biasio, A. US in mid-portion Achilles tendon injury. *J. Ultrasound* **17**, 135–139 (2014).
40. Franz, J. R., Slane, L. C., Rasske, K. & Thelen, D. G. Non-uniform in vivo deformations of the human Achilles tendon during walking. *Gait Posture* **41**, 192–197 (2015).

Content courtesy of Springer Nature, terms of use apply. Rights reserved

41. Komi, P. V., Fukashiro, S. & Järvinen, M. Biomechanical loading of Achilles tendon during normal locomotion. *Clin. Sports Med.* **11**, 521–531 (1992).
42. Lichtwark, G. A. & Wilson, A. M. In vivo mechanical properties of the human Achilles tendon during one-legged hopping. *J. Exp. Biol.* **208**, 4715–4725 (2005).
43. Obst, S. J., Newsham-West, R. & Barrett, R. S. Changes in Achilles tendon mechanical properties following eccentric heel drop exercise are specific to the free tendon. *Scand. J. Med. Sci. Sport.* **26**, 421–431 (2016).
44. Farris, D. J., Trewartha, G., McGuigan, M. P. & Lichtwark, G. A. Differential strain patterns of the human Achilles tendon determined in vivo with freehand three-dimensional ultrasound imaging. *J. Exp. Biol.* **216**, 594–600 (2013).
45. Silbernagel, K. G. & Crossley, K. M. A proposed return-to-sport program for patients with midportion achilles tendinopathy: Rationale and implementation. *J. Orthop. Sports Phys. Ther.* **45**, 876–886 (2015).
46. Nuri, L., Obst, S. J., Newsham-West, R. & Barrett, R. S. Three-dimensional morphology and volume of the free Achilles tendon at rest and under load in people with unilateral mid-portion Achilles tendinopathy. *Exp. Physiol.* **103**, 358–369 (2018).
47. Handsfield, G. G. et al. Achilles subtendon structure and behavior as evidenced from tendon imaging and computational modeling. *Front. Sport. Act. Living* **2**, 70 (2020).
48. Funaro, A., Shim, V., Mylle, I. & Vanwanseele, B. How subject-specific biomechanics influences tendon strains in Achilles tendinopathy patients: A finite element study. *medRxiv* 2024.04.05.24305385 (2024) https://doi.org/10.1101/2024.04.05.24305385.
49. Couppé, C., Svensson, R. B., Josefsen, C. O., Kjeldgaard, E. & Magnusson, S. P. Ultrasound speckle tracking of Achilles tendon in individuals with unilateral tendinopathy: A pilot study. *Eur. J. Appl. Physiol.* **120**, 579–589 (2020).
50. Passini, F. S. et al. Shear-stress sensing by PIEZO1 regulates tendon stiffness in rodents and influences jumping performance in humans. *Nat. Biomed. Eng.* **5**, 1457–1471 (2021).
51. Handsfield, G. G. et al. A 3D model of the Achilles tendon to determine the mechanisms underlying nonuniform tendon displacements. *J. Biomech.* **51**, 17–25 (2017).
52. Pringels, L. et al. Intratendinous pressure changes in the Achilles tendon during stretching and eccentric loading: Implications for Achilles tendinopathy. *Scand. Med. Sci. Sports* **33**, 619–630 (2022).

Acknowledgements
The authors would like to thank the Research Council KU Leuven for providing financial support for this project.

Author contributions
AF, VS, and BV contributed to the conception and design of the study. AF performed volume reconstruction and segmentation, developed the model geometries, performed the free-form deformation, FE modelling and analysis, and statistical analysis. AF wrote the first draft of the manuscript. IM performed muscle force estimation. All authors contributed to manuscript revision and read and approved the submitted version.

Funding
Grant No: C24M/20/053, Research Council KU Leuven.

Declarations

Competing interests
The authors declare no competing interests.

Ethics statement
The studies involving human participants were reviewed and approved by KU/UZ Leuven. The patients/participants provided written informed consent to participate in this study.

Additional information
Supplementary Information The online version contains supplementary material available at https://doi.org/10.1038/s41598-024-84202-9.

Correspondence and requests for materials should be addressed to A.F.

Reprints and permissions information is available at www.nature.com/reprints.

Publisher's note Springer Nature remains neutral with regard to jurisdictional claims in published maps and institutional affiliations.

Open Access This article is licensed under a Creative Commons Attribution-NonCommercial-NoDerivatives 4.0 International License, which permits any non-commercial use, sharing, distribution and reproduction in any medium or format, as long as you give appropriate credit to the original author(s) and the source, provide a link to the Creative Commons licence, and indicate if you modified the licensed material. You do not have permission under this licence to share adapted material derived from this article or parts of it. The images or other third party material in this article are included in the article's Creative Commons licence, unless indicated otherwise in a credit line to the material. If material is not included in the article's Creative Commons licence and your intended use is not permitted by statutory regulation or exceeds the permitted use, you will need to obtain permission directly from the copyright holder. To view a copy of this licence, visit http://creativecommons.org/licenses/by-nc-nd/4.0/.

© The Author(s) 2025

Content courtesy of Springer Nature, terms of use apply. Rights reserved

Terms and Conditions

Springer Nature journal content, brought to you courtesy of Springer Nature Customer Service Center GmbH (“Springer Nature”).
Springer Nature supports a reasonable amount of sharing of research papers by authors, subscribers and authorised users (“Users”), for small-scale personal, non-commercial use provided that all copyright, trade and service marks and other proprietary notices are maintained. By accessing, sharing, receiving or otherwise using the Springer Nature journal content you agree to these terms of use (“Terms”). For these purposes, Springer Nature considers academic use (by researchers and students) to be non-commercial.
These Terms are supplementary and will apply in addition to any applicable website terms and conditions, a relevant site licence or a personal subscription. These Terms will prevail over any conflict or ambiguity with regards to the relevant terms, a site licence or a personal subscription (to the extent of the conflict or ambiguity only). For Creative Commons-licensed articles, the terms of the Creative Commons license used will apply.
We collect and use personal data to provide access to the Springer Nature journal content. We may also use these personal data internally within ResearchGate and Springer Nature and as agreed share it, in an anonymised way, for purposes of tracking, analysis and reporting. We will not otherwise disclose your personal data outside the ResearchGate or the Springer Nature group of companies unless we have your permission as detailed in the Privacy Policy.
While Users may use the Springer Nature journal content for small scale, personal non-commercial use, it is important to note that Users may not:

1. use such content for the purpose of providing other users with access on a regular or large scale basis or as a means to circumvent access control;
2. use such content where to do so would be considered a criminal or statutory offence in any jurisdiction, or gives rise to civil liability, or is otherwise unlawful;
3. falsely or misleadingly imply or suggest endorsement, approval , sponsorship, or association unless explicitly agreed to by Springer Nature in writing;
4. use bots or other automated methods to access the content or redirect messages
5. override any security feature or exclusionary protocol; or
6. share the content in order to create substitute for Springer Nature products or services or a systematic database of Springer Nature journal content.

In line with the restriction against commercial use, Springer Nature does not permit the creation of a product or service that creates revenue, royalties, rent or income from our content or its inclusion as part of a paid for service or for other commercial gain. Springer Nature journal content cannot be used for inter-library loans and librarians may not upload Springer Nature journal content on a large scale into their, or any other, institutional repository.
These terms of use are reviewed regularly and may be amended at any time. Springer Nature is not obligated to publish any information or content on this website and may remove it or features or functionality at our sole discretion, at any time with or without notice. Springer Nature may revoke this licence to you at any time and remove access to any copies of the Springer Nature journal content which have been saved.
To the fullest extent permitted by law, Springer Nature makes no warranties, representations or guarantees to Users, either express or implied with respect to the Springer nature journal content and all parties disclaim and waive any implied warranties or warranties imposed by law, including merchantability or fitness for any particular purpose.
Please note that these rights do not automatically extend to content, data or other material published by Springer Nature that may be licensed from third parties.
If you would like to use or distribute our Springer Nature journal content to a wider audience or on a regular basis or in any other manner not expressly permitted by these Terms, please contact Springer Nature at

onlineservice@springernature.com